Phase Separation of Several Kinds of Polyethylene Solution under the Gelation/Crystallization Process

Masaru Matsuo,*,† Seiko Miyoshi,† Mami Azuma,† Yuezhen Bin,† Yasuyuki Agari,‡ Yuufu Sato,§ and Akihito Kondo§

Department of Textile and Apparel Science, Faculty of Human Life and Environment, Nara Women's University, Nara 630-8263, Japan; Oosaka Municipal Technical Research Institute, Osaka 536-8553, Japan; and Peterochemical Resarch Laboraory, Sumitomo Chemical Co., Ltd., 2-1 Kitasoda Sodegaura-City, Chiba Pref 299-0295, Japan

Received February 10, 2005

ABSTRACT: The gelation mechanism of polyethylene solutions was investigated by using light scattering and X-ray diffraction techniques in terms of the liquid−liquid phase separation. Three kinds of polyethylene, ultrahigh molecular weight polyethylene (UHMWPE), low molecular weight linear polyethylene (L-LMWPE), and low molecular weight branched polyethylene (B-LMWPE), were used as test specimens. When an incident beam of He−Ne gas laser was directed to the UHMWPE and B-LMWPE solutions quenched to a desired temperature, the logarithm of scattered intensity increased linearly in the initial stage and tended to deviate from this linear relationship in the latter stage. If the linear increase in the initial stage can be analyzed within the framework of the linear theory of spinodal decomposition proposed by Cahn, the gelation is obviously attributed to the phase separation leading to the concentration fluctuation of the solution. Furthermore, in the later stage showing the deviation from the linear relationship, light scattering from the UHMWPE solution with 0.5% concentration under Hv polarization condition showed an X-type pattern, indicating the appearance of optically anisotropic rods. On the other hand, the scattering from the B-LMWPE solution with 3% concentration showed a four-leaf clover pattern, indicating the appearance of optically anisotropic spherulites. No crystallite was confirmed by the X-ray diffraction measurements, when the rods and spherulites appeared. With further lapse of time, the Hv patterns became clearer and the corresponding X-ray diffraction intensity curves showed a very small diffraction peak from the (110) plane. In contrast, for the L-LMWPE solutions, the logarithm of scattered intensity against time showed a rapid increase and tended to level off because of rapid change from slightly transparent to whiten gels. In such a process, any quantitative analysis of the scattered light intensity was impossible. The corresponding X-ray diffraction revealed the strong reflections from the (110) and (200) planes, indicating the rapid formation of stable crystallites. Through a series of experiments for the three kinds of polyethylene solution, it turned out that gelation mechanism of polyethylene solutions is strongly affected by molecular weight and the degree of branching.

Introduction

Polymer chains usually form an interconnected network that gives rise to characteristic texture and properties, in the interstice of which are molecules of solvent and other species. Of course, gel formation involves association of chain segments, resulting in a three-dimensional framework that contains solvent in the interstices. The associated regions are known as junction zones and may be formed from two or more chains.

Recent improvements have led to a number of new insights for the investigation of gelation mechanism. One of the typical physical gels of linear polymers has been observed for atactic (at-), isotactic (it-), and syndiotactic (st-) polystyrene (PS).[1−10] Gel structure and dynamics of it-PS and st-PS have been investigated in their equilibrium states. The studies of it-PS have been carried out by using decalin as solvent to analyze the coagulation structure as well as the conformation of an isolated chain in gels relating to the 3_1 helix. Kobayashi et al.[1−3] pointed out that there exist long chains with TTGG conformation within st-PS gels at room temperature and proposed the further analysis of st-PS gels prepared by several solvents on the basis of the results of Kratky plots and time dependence of invariant of the small-angle neutron scattering data. As the results, it was found that the molecular coagulation process is sensitive to the kinds of solvent.

Apart from a series of the investigations,[1−10] Prins et al. studied the gelation mechanism of agarose on the basis of the time dependence of scattered intensity of He−Ne gas laser from the gels prepared by quenching solutions.[11,12] According to their experiment,[11] the logarithm plots of the scattered intensity against time at only one fixed scattering angle showed a straight line, as has been observed for the phase separation of amorphous blend films.[13] They concluded that the initial gelation of agarose is due to the liquid−liquid phase separation associated with spinodal decomposition. Certainly, their paper for agarose[12] was the first proposal that the gelation is associated with the liquid−liquid phase separation, although their investigation for agarose was only the suggestion. Since then, more detailed analysis has been reported for several kinds of polymers.[14−18]

Namely, the gelation mechanism of polymer solutions by quenching has been studied for poly(vinyl alcohol) (PVA) with intra- and intermolecular hydrogen bonds by Kanaya et al.[14] using wide- and small-angle neutron scattering and by Matsuo et al.[15,16] using X-ray diffrac-

† Nara Women's University.
‡ Oosaka Municipal Technical Research Institute.
§ Sumitomo Chemical Co., Ltd.
* To whom all correspondence should be addressed: Tel and Fax 81-742-20-3462; e-mail m-matsuo@cc.nara-wu.ac.jp.

10.1021/ma058003p CCC: $30.25
Published on Web 06/28/2005

Table 1. Characterizations of the Three Kinds of Polyethylene

method	subjects	G201	Sholex 4551	UHMWPE
^{13}C NMR	degree of short chain branching (SCB, 1/1000C)	19	1	<1
	ethyl branching	4.5 ± 0.5	1	
	buthyl branching	8.8		
	amiru branching	2.3		
	hexyl branching	3.5		
GPC	$\bar{M}_w$	260000	221000	2190000
	$\bar{M}_n$	25400	29600	51900
	$\bar{M}_w/\bar{M}_n$	10.2	7.5	4.2
TREF	elusion temp(°C)	73	98	101
GPC−light scattering	$\bar{M}_w$	1240000	223000	2200000
GPC−viscosity	$g^* = [\eta]_s/[\eta]_l$	0.43	1	1

tion, small-angle light scattering (SALS) under Hv and Vv polarization conditions, and scanning electron microscopy (SEM). Further detailed studies have been carried out by Matsuo et al. for ultrahigh molecular weight polypropylene (UHMWPP)[17] based on light scattering, X-ray, infrared, and Raman measurements. Through a series of experimental results, Matsuo et al. provided conclusive evidence that when crystalline polymer solutions are quenched, the liquid−liquid phase separation associated with spinodal decomposition occurs at first, and the crystallization occurs subsequently in the polymer-rich phase. Especially, phase separation of the UHMWPP solution in the gelation process was investigated in relation to the morphology and mechanical properties of the resultant dry gel film. They pointed out that the dense network structure plays an important role in ensuring significant drawability in order to transmit inner stress smoothly in the stretching direction. The phase separation in the gelation process was studied by light scattering technique to facilitate understanding of the formation of such network structure. Despite the detailed analysis for the UHMWPP,[17] the time dependence of crystallite formation after rapid temperature dropping could not be measured by X-ray diffraction, although the estimation is very important to study whether the gelation is attributed to the phase separation of solution by the concentration fluctuation.

This paper mainly deals with gelation mechanism of the ultrahigh molecular weight polyethylene (UHMWPE) and the branched low molecular weight polyethylene (B-LMWPE) solutions by X-ray and He−Ne gas laser in terms of time dependence of crystallite formation leading to the phase separation of the solutions. However, any analysis has never been reported for polyethylene in terms of the phase separation based on the concentration fluctuation by spinodal decomposition because of the difficulty in measuring the changes in light scattering intensity and X-ray diffraction intensity with elapsing time due to very rapid crystallization. Actually, the scattered light intensity from the UHMWPE and B-LMWPE solutions could be detected by photodiodes set at desired scattering angles, when the blend solutions of the UHMWPE and B-LMWPE were quenched at temperatures lower than their gelation temperatures. To obtain the reliable results, repeated experiments have been done to check the reproducibility. On the basis of the period of the change from the transparent to whiten gel, the kinetics of the gelation mechanism could be analyzed in view of phase separation of the solutions. Furthermore, the time-resolved X-ray diffraction technique was used to support the above phenomena obtained by a He−Ne gas laser. Incidentally, as described later, the analysis for L-LMWPE solutions was impossible because of a very rapid change from the solution to whiten gel.

Another background of the present work is due to ultradrawing of blend films of UHMWPE and LMWPE prepared by gelation/crystallization from solution. The purpose is to prepare high modulus and high strength fibers with commercially interesting speed, since the viscosity of solution undergoes a drastic decrease with increasing content of LMWPE.[19−21] Certainly, the excellent work by Smith and Lemstra[22−24] for ultradrawing of UHMWPE films has caused big impacts to the industrial field of polymer science, and a number of improvements have been done in terms of industrial level. According to our previous works,[19−21] UHMWPE and B-LMWPE blend films, the B-LMWPE content being 50%, could be elongated up to 200 times and the Young's modulus reached 76.5 GPa, while the maximum draw ratio of UHMWPE and L-LMWPE blend films was up to 30 times and the surface of the drawn film was not uniform due to poor miscibility and the further elongation caused the breaking holes within the film. This is probably thought to be due to the fact that gelation mechanism is sensitive to the molecular weight and the degree of branching. Then three commercial polyethylene samples are adopted in the present work.

Experimental Section

Sample Characterizations. Three kinds of polyethylene, Hercules 1900/90189 with ultrahigh molecular weight, Sholex 4551, and Sumikasen G201, were used as test specimens. They have used widely in the industrial fields to produce fibers and films. Hercules 1900/90189, Sholex 4551, and Sumikasen G201 are known as ultrahigh molecular weight polyethylene (UHMWPE), low molecular weight linear polyethylene (L-LMWPE), and low molecular weight branched polyethylene (B-LMWPE). The detailed characterizations of the three kinds of polyethylene were carried out before gelation/crystallization measurements.

The degree of short chain branching as well as the kinds of branching for three kinds of polyethylene was estimated from the results by ^{13}C NMR[25] (AVANC600 of Bruker Co. Ltd.) at 135 °C. The measurements were done by using a sample tube of 10 mm i.d., and the accumulation number was 1200−22000. The solvent was *o*-dichlorobenzene containing very small amounts of butylated hydroxytoluene as stabilizer, and the concentrations of solutions were 0.2−5 wt %. The results are listed in Table 1.

To estimate the branching degree of short chains, the temperature rising elution fractionation (TREF) method was adopted. In doing so, polyethylene was poured into a column, 21 mm i.d. × 150 mm, containing glass beads with 0.15−0.17 mm diameter, at 145 °C. As solvent, *o*-dichlorobenzene containing very small amounts of butylated hydroxytoluene as a stabilizer was used. The column temperature undergoes from 145 to −10 °C slowly and upturn from −10 to 145 °C; as cooling process, (1) 0.5 °C/min from 145 to 120 °C, (2) 0.25 °C/min

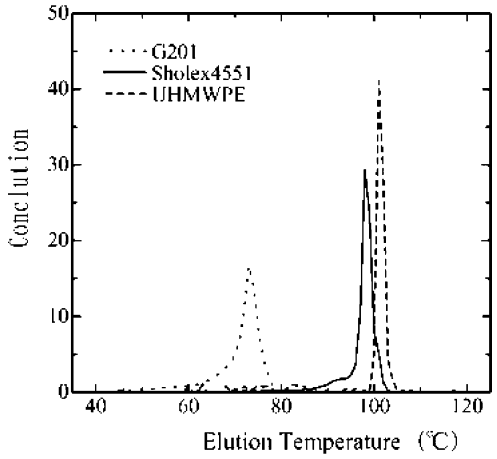

Figure 1. Distribution curves of the short chain branching for three kinds of polyethylene, G201 (B-LMWPE), Sholex 4551 (L-LMWPE), and Hercules 1900/90189 (UHMWPE), estimated by the TREF method.

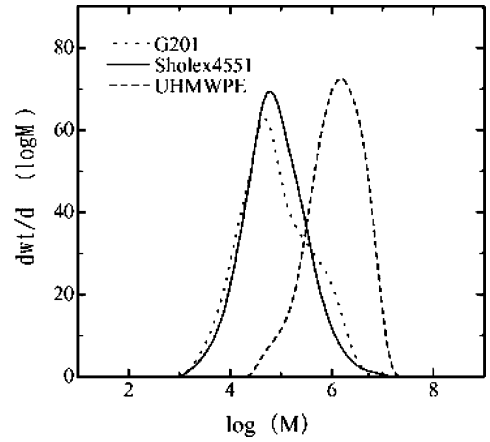

Figure 2. Molecular weight distribution curves for three kinds of polyethylene, G201 (B-LMWPE), Sholex 4551 (L-LMWPE), and Hercules 1900/90189 (UHMWPE), measured by GPC analysis.

from 120 to −10 °C, and (3) keeping for 2 h at −10 °C, and as heating process, (1) 0.25 °C/min from −10 to 120 °C and (2) 0.5 °C/min from 120 to 145 °C. The resolved polyethylene was detected at every 1 °C interval by infrared (IR), and the absorption area of the IR spectrum between 2980 and 2810 cm^{-1} was postulated as polymer concentration.[26] The distribution of short chain branching is shown in Figure 1. The elusion temperatures corresponding to the highest concentration for each resolved polyethylene are listed in Table 1.

To estimate apparent $\bar{M}_n$ (the average number of molecular weight) and $\bar{M}_w$ (the average weight of molecular weight), GPC analysis was done by using HLC-8121GPC/HT (Toso Co. Ltd.) with refraction index (RI) detector at 152 °C. As solvent, *o*-dichlorobenzene containing very small amounts of butylated hydroxytoluene as a stabilizer was used, and the concentration of solutions was 0.05 wt %. TSK standard polystyrenes, F850 to A-1000 (Toso Co. Ltd.), with molecular weight range from 1000 to 8400000 g/mol, were adopted as the standard specimens to determine $\bar{M}_n$ and $\bar{M}_w$ relatively, on the basis of a standard curve. The analyzed molecular weights were calculated as a linear polyethylene by using *Q* factors (molecular weight against 1 Å) of polyethylene and polystyrene given to be 41.3 and 17.7, respectively.[27] Figure 2 shows the results. The three curves indicated that polyethylene specimens used in this experiment have a broad distribution of molecular weight, and the obtained relative values of $\bar{M}_n$ and $\bar{M}_w$ are listed in Table 1.

In addition to the above relative estimation, the absolute values of $\bar{M}_w$ were estimated at 145 °C by light scattering (PD2040 of Precision Co. Ltd.), used as a detector of GPC (HLC-8110). As solvent, 1,2,4-trichlorobenzene containing very small amounts of butylated hydroxytoluene as a stabilizer was used, and the concentration of solutions was 0.1−0.03 wt %. The columns are TSK gel GMHHR-H(20) with 7.8 mm i.d. × 30 cm. TSK standard polystyrene, F-4, with $\bar{M}_w = 37\,900$ (Toso Co. Ltd.) was used to obtain the equipment constant and standard reference material-1483 ($\bar{M}_w = 32\,100$ and $\bar{M}_w/\bar{M}_n = 1.1$) obtained from the National Institute of Standard and Technology (NIST) was used to correct the values obtained by light scattering instrument. The absolute values of $\bar{M}_w$ are listed in Table 1. The GPC on-time viscometer measurement was carried out by GPC equipped with a 210 differential viscometer (Viscotek Co. Ltd.) to estimate the degree of long chain branching indirectly. In doing so, the viscosity ($[\eta]_s$) of the specimens and the viscosity ($[\eta]_l$) of the standard reference material 1475a ($\bar{M}_w = 52000$, $\bar{M}_w/\bar{M}_n = 2.9$) obtained from NIST were obtained, and $g^* = \{[\eta]_s\}/\{[\eta]_l\}$ was determined.[28] They are also listed in Table 1.

As listed in Table 1, Sumikasen G201 is the branched polyethylene, while Sholex 4551 and UHMWPE are the linear polyethylenes. The GCP result in Figure 2 reveals that the molecular distributions of the three kinds of polyethylene are wide polydisperse. As for the results of $\bar{M}_w$, the molecular weight measurements are thought to be highly reliable. The values of g^* indicate no long chain branching of Sholex 4551 and UHMWPE, while the conclusive evidence for Sumikasen G201 cannot be obtained from the g^* value, 0.43, because of a number of short chain branching. In the following discussion, Hercules 1900/90189, Sholex 4551, and Sumikasen G201 are termed as UHMWPE, L-LMWPE, and B-LMWPE, respectively.

Sample Preparation. The solutions with various concentrations were prepared by heating the well-blended polymer/solvent mixture at 150 °C for 30 min. The solvent was decalin. They were put in each test tube and kept at 85 °C for 5 min to avoid a drastic convection. After that, the test tube was immediately set in a time-resolved light scattering instrument to measure time dependence of scattered light intensity by using He−Ne gas laser. In this instrument, 10 photodiodes were set at the desired scattering angle in order to detect the scattering beam at various angles simultaneously. Such time-resolved light scattering measurements were done at desired temperatures beyond 65 °C for the UHMWPE solutions and beyond 40 °C for the B-LMWPE solutions. The diameter of light scattering cell tube was 10 mm to maintain an equilibrium state in solution ensuring the construction of ergodic hypothesis.

To determine the gelation temperature, the test tube containing the solution was tilted after standing 1 h in a water bath at a constant temperature. When the meniscus deformed but the specimen did not flow under its own weight, we judged that the solution had gelled. The lowest temperature at which the onset of gelation occurred within 1 h was defined as the gelation temperature. This is similar to the method used in the previous papers.[15−18] On the other hand, another method was adopted to determine the gelation time at a fixed temperature. The estimation was carried out by using the so-called "falling-ball method". In this estimation, the weight and diameter of a small steel ball were 30 mg and 2 mm, respectively. When the solution was set at a fixed temperature, the ball was put on the surface of the solution at a proper time interval. When a ball was kept on the surface by the gelation of solution progressed with elapsing time, the time was defined as "gelation time".[18]

Small-angle light scattering (SALS) under cross-polarization (Hv) conditions was observed with a 15 mV He−Ne gas laser as a light source.

The X-ray measurements were carried out with a 12 kW rotating-anode X-ray generator (Rigaku RDA-rA) operated at 150 mA and 40 kV. The X-ray beam using Cu Kα radiation was monochromatized with a curved graphite monochromator. The diameter of an X-ray cell tube was 1 mm. Time resolution of WAXD intensity was done to study gelation mechanism by using a curved position-sensitive proportional counter (PSPC)

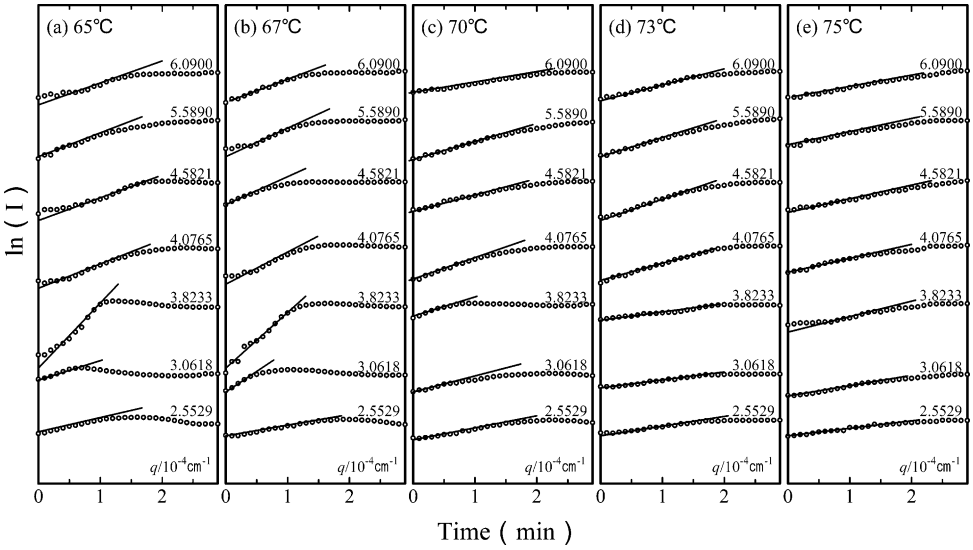

Figure 3. Logarithm plots of the scattered intensity against time at various q observed for the 0.3% UHMWPE solution.

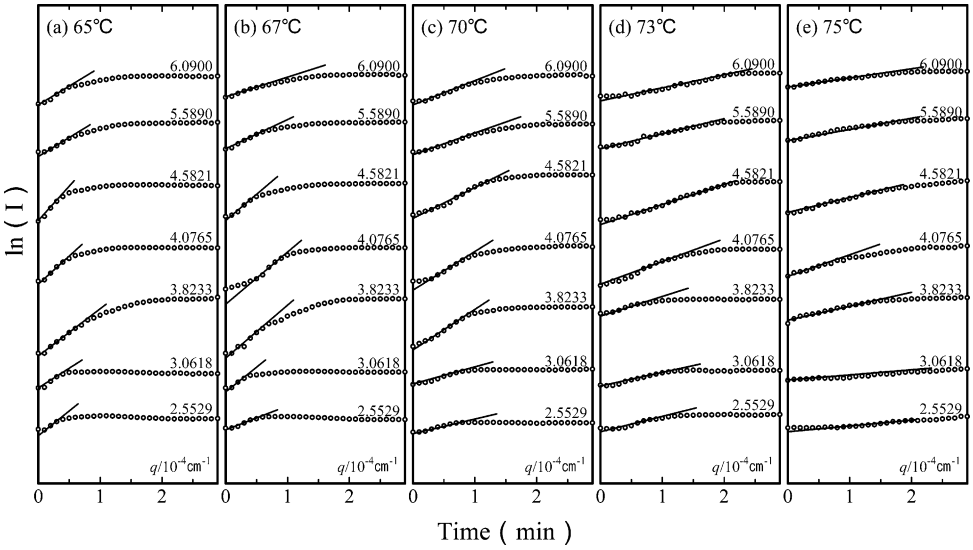

Figure 4. Logarithm plots of the scattered intensity against time at various q observed for the 0.5% UHMWPE solution.

to estimate the change in diffraction intensity distribution as a function of the Bragg angle simultaneously. The sample preparation was done by a procedure similar to the light scattering measurement.

DSC measurements were performed with an Exstar 6000 of Seiko Instrument Inc. The experiments were done to study the gelation/crystallization process under cooling process of solutions. In this experiments, gel was packed in a sample pan and was heated to 150 °C. The cooling rate was 1 °C/min. In the sample pan, gel was packed without any space.

Results and Discussion

Light Scattering. Figures 3 and 4 show the change in the logarithm plots of the scattered intensity against time (t) at various q observed for 0.3 and 0.5% UHMWPE solutions. The magnitude of the scattered vector, q, is given by $q = (4\pi n/\lambda')\sin(\theta/2)$, where λ', θ, and n are the wavelength of light in solution, the scattering angle, and the refractive index of the solvent, respectively. The measurements were done in the temperature range from 65 to 75 °C. The logarithm of the scattered intensity, $\ln(I)$, increases linearly with time in the initial stage of phase separation of the solution and tends to deviate from the linear relationship. The deviation shifts to shorter time scale, and the slope of the linear line becomes sharper as temperature decreases. If the linear relationship is related to liquid−liquid phase separation of the solution, the appearance of slightly opaque UHMWPE gel must be independent of the crystallization. To check this, the measurements for small-angle light scattering under Hv polarization condition and X-ray diffraction were carried out. Of course, the similar tendency was observed for the 0.4% solution.

Figure 5 shows the change in Hv pattern against time measured for the 0.3% solutions at 65 °C. Hv scattering cannot be observed at 45 s corresponding to the time scale ensuring the straight line of $\ln(I)$ vs t, which indicates no appearance of superstructures as aggregation of quasi-crystallites much smaller than the wavelength of the incident beam. With time, the plots of $\ln(I)$ vs t deviates from the straight line and the corresponding Hv scattering shows a X-type pattern, indicating the existence of optically anisotropic rodlike textures, the optical axes being oriented parallel or perpendicular to the rod axis.[29] With the further lapse of time, the pattern becomes more distinct, indicating an increase in the number of rods associated with the gradual development of gelation. The scattered intensity is similar to that from polymer films and is much stronger

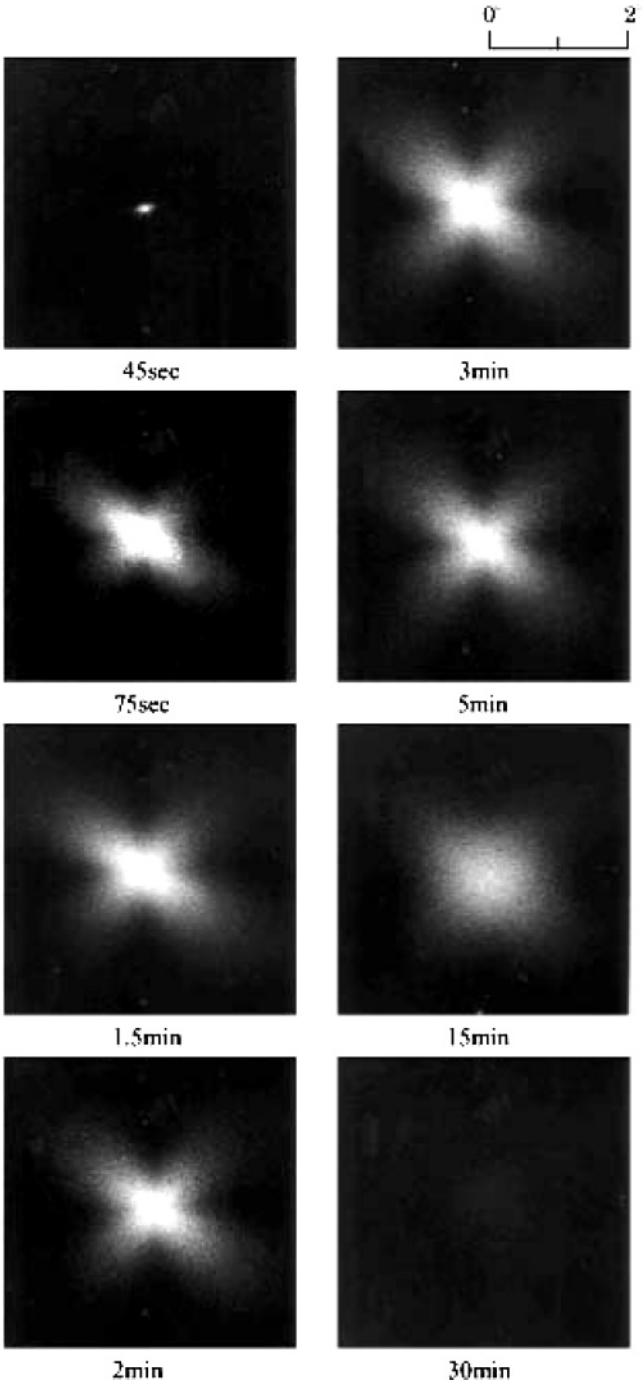

Figure 5. Change in Hv pattern against time measured for the 0.3% UHMWPE solution at 65 °C.

than that from poly(vinyl alcohol) gels[15,16] and agarose gels.[18] This is due to the higher ordering of optical axes, corresponding to molecular chains, with respect to the rod axis as well as large difference of the optical density fluctuation between the rods and the medium in the UHMWPE solutions. However, the scattering pattern became indistinct beyond 15 min and finally disappeared with further elapsing time. The same phenomenon was also observed for the 0.4 and 0.5% solutions, although the appearance of the X-type pattern became faster with increasing the concentration. The disappearance is obviously attributed to be a random orientation of the optical axes with respect to the rod axis, but the reason remains unresolved problem. Even so, it may be speculated that appearance of a number of rods with the progression of the gelation causes collision between isolated rods and the disruption of each rod by the collision probably disturbs the ordered orientation of the optical axes with respect to the rod axis.

Of course, the structures could be observed under optical microscopy and polarized microscopy, but the structures are too distinct to discern as rodlike textures. After 15 min, the structures tended to disappear, and polarized microscopy showed a dark area.

Figure 6 shows the change in the logarithm plots of the scattered light intensity against time at various q observed for the 5.0% B-LMWPE solution. As can be observed for the UHMWPE solution (see Figures 3 and 4), the logarithm of the scattered intensity, $\ln(I)$, also increases linearly with time in the initial stage of the phase separation of the solution and tends to deviate from the linear relationship. The deviation shifts to shorter time scale as the temperature decreases. The same tendency was also observed for the 3 and 4% solutions.

Returning to Figures 3, 4, and 6, it is seen that the time scale ensuring the linear relationship is much shorter than those of the other polymer solutions such as PVA,[15,16] UHMWPP,[17] and arogose.[18] This indicates the difficulty in measuring the growth rate of the concentration from the slope of the linear line, which shall be discussed later. The measurements concerning Figures 3, 4, and 6 were carried out several times (more than three times). Even so, some lines drawn from the plots are not credible; the slope at $q = 4.0765$ at 67 °C in Figure 3, those at $q = 4.5821$ at 65 °C and at $q = 3.8233$ at 75 °C in Figure 4, and those at $q = 3.0618$ and 3.8233 at 45 °C in Figure 6. The several repeated measurements provide that the drawing the plotted points ensures a linear line, but even so some points deviate from the line described above. The best results are shown in Figures 3, 4, and 6. Such difficult experiments are due to a shorter interval, ensuring a linear relationship in comparison with other crystalline polymer solutions such as PVA,[15,16] UHMWPP,[17] and agarose[18] as discussed above, and then a detailed investigation of gelation mechanism of UHMWPE solutions has never been reported.

Figure 7 shows the change in Hv pattern against time measured for the 5% solutions at 65 °C. No Hv pattern is observed at 5 min associated with the deviation from the linear relationship of $\ln(I)$ vs time. This indicates no formation of a random array of quasi-crystallites smaller than the wavelength of the incident beam. With elapsing time, the corresponding Hv scattering shows a four-leaves clover pattern, verifying the appearance of optically anisotropic spherulites.[30] With further elapsing time, the pattern becomes more distinct, indicating an increase in the number of spherulites with the gradual development of gelation. The pattern was maintained beyond 3 h, which was different from time scale concerning the Hv scattering from the UHMWPE gels (see Figure 5).

X-ray Diffraction. A question can be arisen as to whether quasi-crystallites with unstable crystal lattice were performed in the rods and/or spherulites. To check this phenomenon, X-ray diffraction intensity was measured as a function of time, when the UHMWPE solution at 150 °C was quenched to the desired temperatures immediately. Figure 8 shows the results for the 0.5% solution. The curve at 0 min denotes the accumulation of intensity in the range from 0 to 400 s,

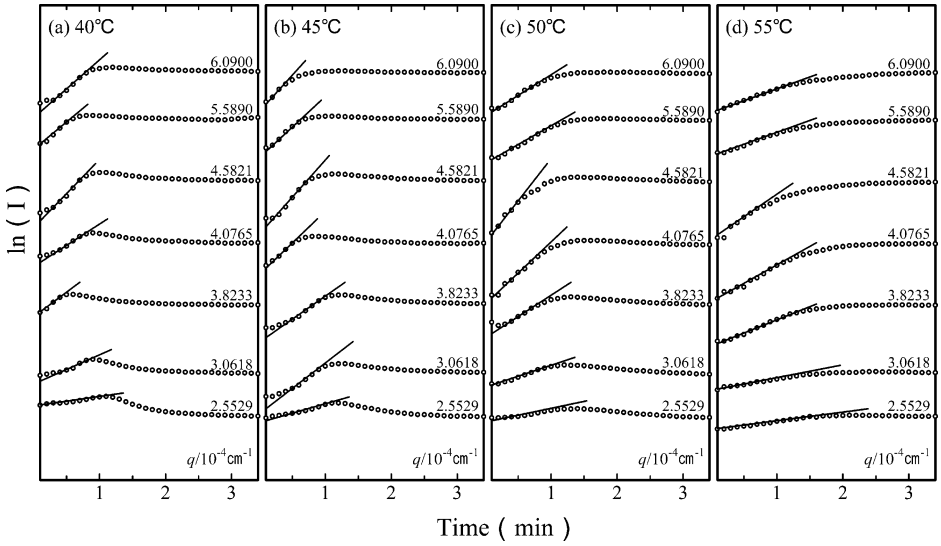

Figure 6. Logarithm plots of the scattered intensity against time at various q observed for the 5.0% B-LMWPE solution.

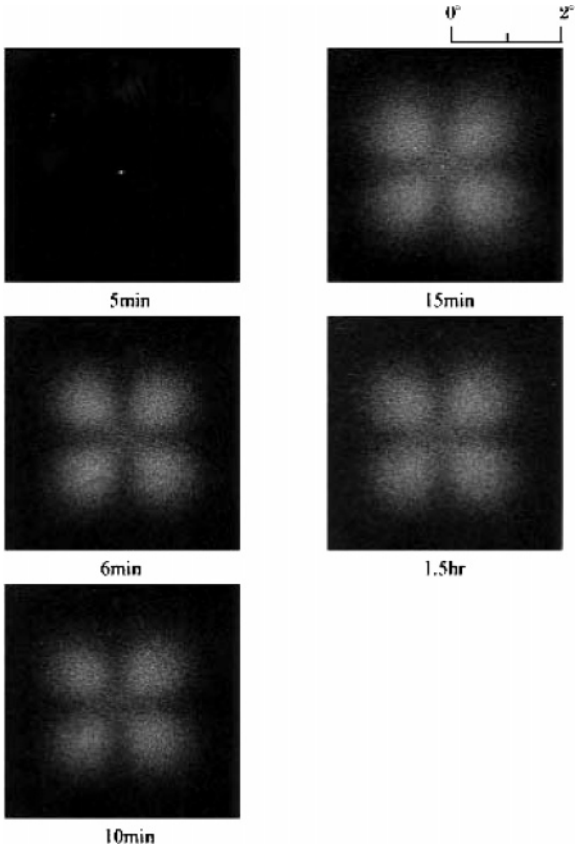

Figure 7. Change in Hv pattern against time measured for the 5% B-LMWPE solution at 65 °C.

since the accumulation period must be taken to be 400 s ensuring smooth diffraction curves. The observation reveals that the crystallization by the rapid temperature drop to 70 °C was not apparently confirmed within 400 s, indicating no crystallization in the initial stage ensuring a linear increase in ln(I) against time. The X-ray intensity shows very small peaks from the (110) and (200) planes of unstable crystallites leading to the ordering of molecules beyond 400 s, which indicates formation of quasi-crystallites as detected by X-ray diffraction. The peak from the (200) plane becomes slightly clearer with time, indicating the growth of crystallites. Furthermore, a very small peak from the (110) plane at 90 °C occurred in the time range 800−1200 s. Any crystallization, however, did not occur at 100 °C (not shown in this paper). The measurements could not be carried out for the solutions whose concentrations were beyond 0.4%. Because of a drastic increase in viscosity of the solution by a slight increase in the concentration, it was impossible to pour the solutions with concentration higher than 0.5% into an X-ray cell (1 mm diameter).

Figure 9 shows the time dependence of X-ray diffraction intensity from the B-LMWPE (G201) solutions, in which the intensity distributions from the 3% solution in columns (a) and (b) were measured at 20 and 60 °C, respectively, and the distributions from the 5% solution in columns (c) and (d) were measured at 20 and 60 °C, respectively. The time dependence at 40 °C (not shown in this paper) was confirmed to be similar to that at 60 °C rather than at 20 °C. Of course, the curve at 0 min also denotes the accumulation time of intensity in the range from 0 to 400 s.

When the solution was quenched to 20 °C, the diffraction curve in the time scale 0−400 s shows a very small peak from the (110) plane. Beyond 800 s, the peak in the curve shows the same magnitude, indicating saturation of the crystallization. Actually, the rapid gelation was confirmed when quenching the solution to 20 °C. For the 5% solution at 20 °C, the very small peak from the (200) plane is observed in addition to the peak from the (110) plane, indicating the formation of stable crystallites. On the other hand, the peak from the solution quenched to 60 °C becomes slightly higher with elapsing time, reflecting gradual crystallization with time. Anyway, it is evident that no crystallization occurred in the initial stage (0−120 s) ensuring the linear relationship of ln(I) vs t in Figure 6.

Despite the similar phenomena measured for the UHMWPE and B-LMWPE solutions, the gelation mechanism of the L-LMWPE solutions was quite different from those of the both solutions. The change in the logarithm plots of the scattered intensity against time at various q could not be observed for the L-LMWPE because of rapid change to whiten solutions by cooling. Hence, X-ray diffraction intensity from the 3% solutions at 20 and 80 °C is only shown in Figure 10. In the time period 0−400 s, the diffraction peaks from the (110) and the (200) planes could be observed clearly, indicating

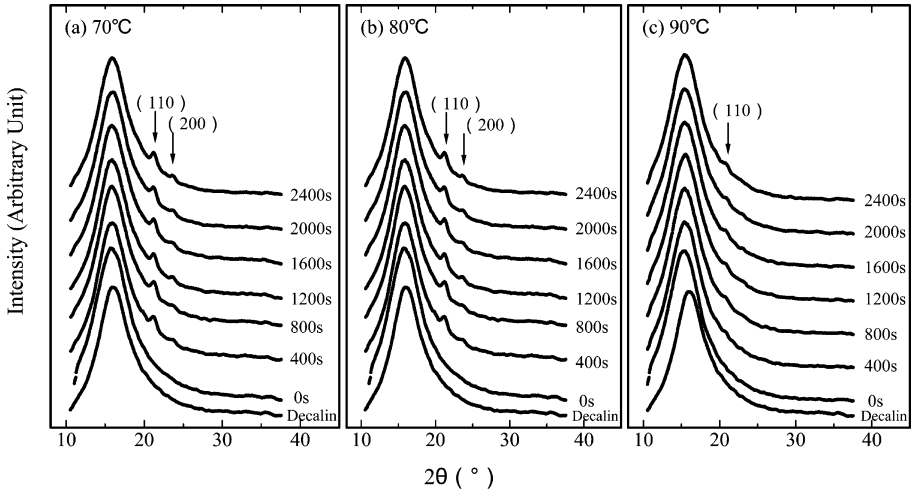

Figure 8. (a) X-ray diffraction intensity from the 0.5% UHMWPE solution quenched to 20 °C. (b) X-ray diffraction intensity from decalin solvent at the indicated temperature.

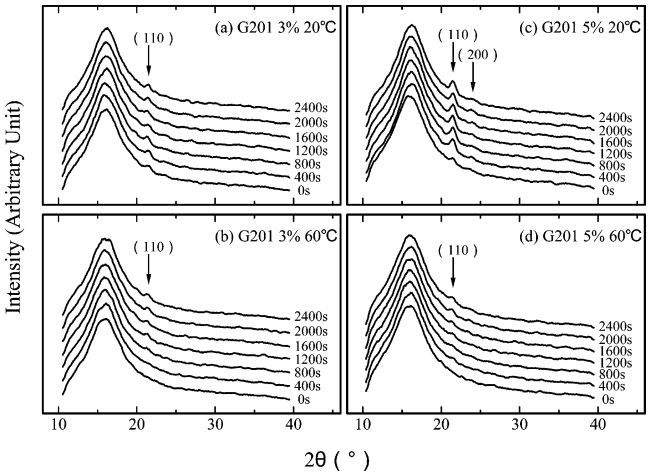

Figure 9. Time dependence of X-ray diffraction intensity from the B-LMWPE (G201) solutions, in which (a) the intensity distributions of 3% solution at 20 °C, (b) the intensity distributions of 3% solution at 60 °C, (c) the intensity distributions of 5% solution at 20 °C, and (d) the intensity distributions of 5% solution at 60 °C.

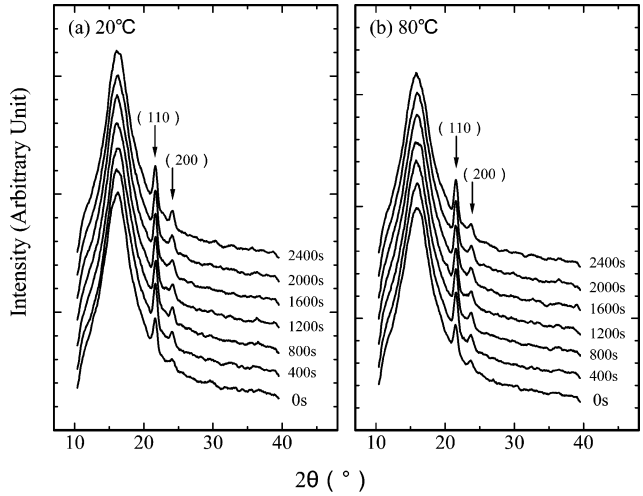

Figure 10. X-ray diffraction intensity observed for the 3% L-LMWPE solutions at 20 and 80 °C.

rapid crystallization even at 80 °C. The rapid appearance is thought to be the instantaneous formation of stable crystallites by quenching the solution, which is independent of the concentration fluctuation in the solution. This behavior is obviously different from the gelation mechanism of the UHMWPE and B-LMWPE solutions discussed before.

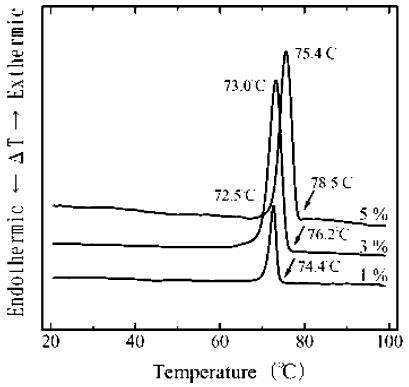

Figure 11. DSC curves for the 3% L-LMWPE solutions under cooling process with cooling rate of 1 °C/min.

The existence of stable crystallites in the L-LMWPE solution was also confirmed by DSC measurements as shown in Figure 11. A very sharp exotherm peak could be observed. The starting temperature of crystallization becomes higher with increasing the concentration of solution, since the ordering of polymer chains becomes easier as the number of chains/volume increases. Anyway, it was impossible to derive the conclusion for gelation mechanism of the L-LMWPE solution based on the present results measured by the X-ray, He−Ne gas laser, and DSC. Accordingly, the following analysis in terms of spinodal decomposition was carried out for the UHMWPE and B-LMWPE solutions. No appearance of crystallites in both solutions was confirmed already in the initial stage ensuring the linear relationship of ln-(I) vs t as shown in Figures 3, 4, and 6.

Here it should be noted that the UHMWPE with linear molecular chains shows the linear relationship indicating the liquid−liquid phase separation of the solution before the gelation, while the crystallization speed of the L-LMWPE is too rapid to detect the relationship. The rapid formation of the L-LMWPE crystallites is thought to be due to fewer entanglements in comparison with the UHMWPE.[31] For the B-LMWPE, many branching hamper the rapid crystallization and provide the linear relationship associated with the phase separation. Through a series of experimental

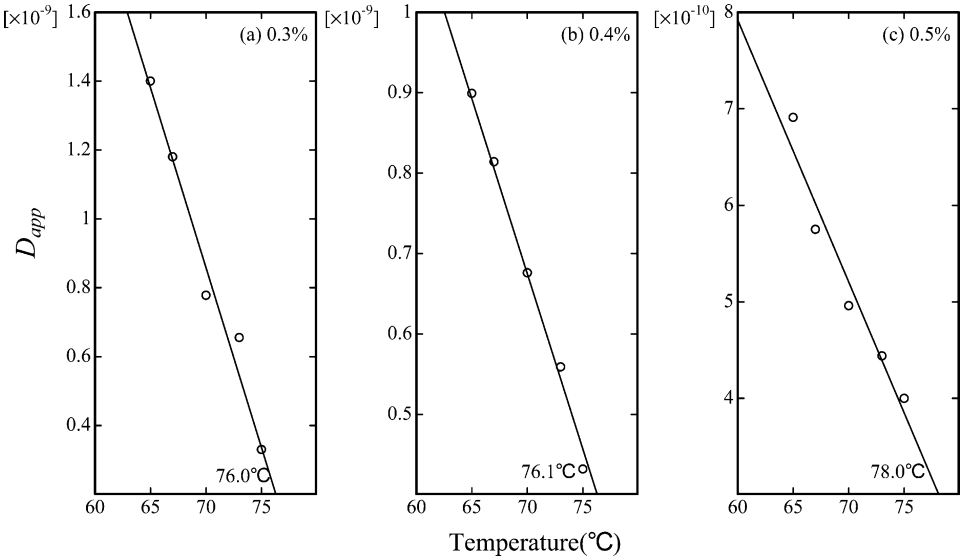

Figure 12. Temperature dependence of D_{app} for the UHMWPE solutions.

results, it turns out that the gelation mechanism is strongly affected by molecular weight and degree of the degree of branching. Incidentally, the crystallinity of the B-LMWPE dry gel was less than 50%, while those of the UHMWPE and the L-LMWPE were higher than 80%.[32]

Analysis of Gelation Mechanism Based on Light Scattering and X-ray Measurements. On the basis of the results in Figures 3−9, it may be concluded that no crystallization occurs in the initial stage of liquid−liquid phase separation of the UHMWPE and B-LMWPE solutions. The deviation of the linear relationship is similar to the later stage of spinodal decomposition as has been observed for amorphous blends.[13] The deviation shifts to shorter time scale as the temperature decreases. Accordingly, the linear increase in ln(I) against time suggests the possibility of successful analysis of the linear theory of spinodal decomposition proposed by Chan.[33] If the linear relationship reflects the initial stage of spinodal decomposition as pointed by Cahn,[33,34] it is well-known that the change in scattered intensity in Figures 3, 4, and 6 can be given by

$$qI(q,t) = I(q,t=0)\exp[2R(q)t] \tag{1}$$

where $I(q,t)$ is the scattered intensity at the time, after initiation of the spinodal decomposition, and $R(q)$ is the growth rate of concentration fluctuation given as a function of q; $R(q)$ is given by

$$R(q) = -D_c q^2\left\{\frac{\partial^2 f}{\partial c^2} + 2\kappa q^2\right\} \tag{2}$$

where D_c is the translational diffusion coefficient of the molecules in solution, f is the free energy of mixing, c is the concentration of solution, and κ is the concentration-gradient energy coefficient defined by Cahn and Hilliard.[34]

To give more conclusive evidence for spinodal decomposition based on the linear relationship, the spinodal temperature T_s was estimated according to the linear theory. In doing so, plots of $R(q)/q^2$ vs q^2 were done at the measured temperature. The plots showed a linear relationship and the apparent diffusion coefficient D_{app}, defined by $D_{app} = -D_c(\partial^2 f/\partial c^2)$, can be obtained by the intercept on the vertical axis.

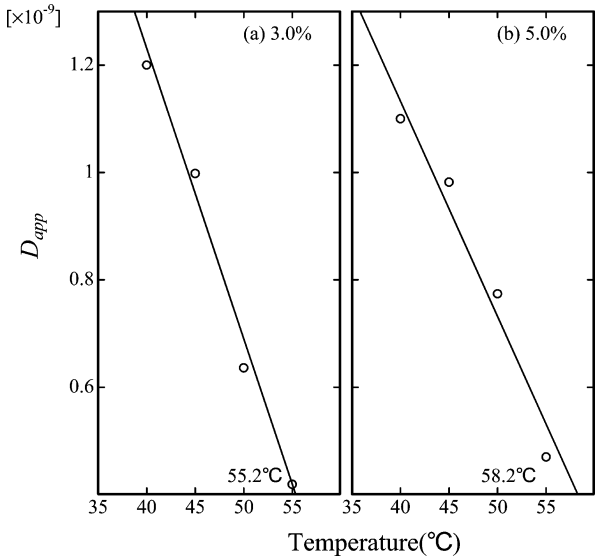

Figure 13. Temperature dependence of D_{app} for the B-LMWPE solutions.

Figures 12 and 13 show the temperature dependence of D_{app} for the UHMWPE and B-LMWPE solutions, respectively. A fairly good linear relationship was also obtained. From the intercept on the temperature axis, one can define the spinodal temperature T_s at $D_{app} = 0$.

Tables 2 and 3 summarize the characteristic parameters describing dynamics of phase separation of the UHMWPE and B-LMWPE solutions, respectively. Among them, the values of $D_{app} = -D_c(\partial^2 f/\partial c^2)$ are significant. Because of the positive values of D_c by definition, the values of $\partial^2 f/\partial c^2$ take a negative value characterizing unstable regions, leading to spinodal decomposition. The small values of $\partial^2 R(q)/\partial q^2|_{q=q_m}$, and hence $D_{app}(\partial^2 R(q)/\partial q^2|_{q=q_m} = 8D_{app})$, indicate no appearance of a scattering maximum of intensity at the initial stage of spinodal decomposition. To observe a distinct scattering maximum in the linear spinodal decomposition regime, it is evident that the value of D_{app} must be usually 2 or 3 orders of magnitude greater.

Here it is seen that the spinodal temperature, T_s, listed in Tables 2 and 3, shifts to higher value as the

Table 2. Values of D_{app} and Spinodal and Gelation Temperatures of the UHMWPE Solutions

(a) Value of D_{app} ($\times 10^{-10}$ cm^2/s)

	concentration (%)		
temp (°C)	0.3	0.4	0.5
65	14.00	8.99	6.91
67	11.80	8.14	5.75
70	7.78	6.76	4.96
73	6.55	5.59	4.44
75	3.30	4.32	4.00

(b) Spinodal and Gelation Temperatures (°C)

concn (%)	SD temp	gelation temp
0.3	76.0	77.0
0.4	76.1	78.2
0.5	78.0	78.5

Table 3. Values of D_{app} and Spinodal and Gelation Temperatures of the B-LMWPE Solutions

(a) Value of D_{app} ($\times 10^{-10}$ cm^2/s)

	concn (%)	
temp (°C)	3.0	5.0
40	13.20	11.00
45	9.98	9.82
50	6.36	7.74
60	4.19	4.70

(b) Spinodal and Gelation Temperatures (°C)

concn (%)	SD temp	gelation temp
3.0	55.2	53.0
5.0	58.2	57.0

concentrations of the UHMWPE and B-LMWPE solutions increase. Interestingly, the values are similar to those of at poly(vinyl alcohol) in dimethyl sulfoxide/water mixtures.[16]

Figure 14 shows the evolution of scattered light intensity of the 0.5% UHMWPE solution plotted against q at the indicated time. The measurements were done at 75 °C slightly lower than spinodal and gelation temperatures. To obtain the quantitative results, the obtained intensity was plotted after subtracting the intensity scattered from the solvent. With elapsing time, the scattering peak becomes higher, but the scattering peak is maintained at the same position. This is surely one of the characteristic phenomena indicating spinodal decomposition. Such a phenomenon was already reported for the gelation of poly(vinyl alcohol),[15,16] polypropylene,[17] and agarose solutions.[18] From the scattering peak, the periodic structure characterizing spinodal decomposition can be estimated to be ca. 1.8 μm by Bragg's equation.

Figure 15 shows the growth rate of concentration $R(q)$ plotted against q estimated for the UHMWPE solutions with 0.3, 0.4, and 0.5% concentrations. The maximum growth rate $R(q_m)$ of the concentration fluctuation increases with decreasing measurable temperature. The scattering vector, q_m, maintains almost the same value of q, independent of the difference ($T_s - T$) between the measured temperature, T, and spinodal temperature, T_s. The same phenomenon was also observed for the B-LMWPE solutions. Such behaviors deviate from the principle of spinodal decomposition for amorphous polymer solutions proposed by van Aartsen.[35] According to his theory, the value of q_m must increase with increasing the difference ($T_s - T$). However, the peak shift of $R(q_m)$ to a higher value of q is too small to recognize the shift clearly. Such a small shift is probably

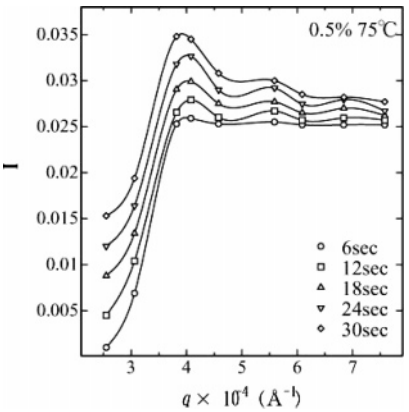

Figure 14. Scattered light intensity of the 0.5% UHMWPE solution plotted against q at the indicated time.

postulated to be the rapid crystallization in the UHMWPE-rich phase formed by spinodal decomposition, but this remains an unresolved problem.

As pointed out before, the slopes in Figures 3, 4, and 6 contain some indistinct factors, since the time interval ensuring each linear slope is much shorter than that for other polymer solutions such as PVA,[15,16] UHMWPP,[17] and agarose.[18] Accordingly, some points in Figures 12, 13, and 15, which are calculated from the slopes in Figures 3, 4, and 6, contain uncertain values, although the best results obtained by the repeated measurements were selected in Figures 3, 4, and 6. Incidentally, we must emphasize that even the values of T_s estimated from another slightly ambiguous experiments were almost the same as the values listed in Tables 2 and 3. This indicates the appropriateness of the present work.

Figures 16 and 17 show DSC curves under the cooling processes measured for the UHMWPE (concentrations, 0.3, 0.4, and 0.5%) and B-LMWPE (concentrations, 1, 3, and 5%) solutions, respectively. All the curves showed an exotherm peak indicating the existence of crystallites. Here it may be noted that despite slow cooling of the solution, the starting temperature to crystallize is almost equal to T_s or less than T_s. This means that phase separation in the solution plays an important role as driving force to cause gelation/crystallization. Of course, the crystallization did not occur when the cooling temperature reached the indicated temperature as shown in Figures 16 and 17 immediately. The speed of rapid temperature drop to estimate spinodal temperature was much faster than 1 °C/min in the present DSC experiment. Actually, the starting point of an exotherm peak shifted to lower temperature with increasing cooling speed.

Returning to Tables 2 and 3, the gelation and spinodal decomposition of the UHMWPE and B-LMWPE solutions occur at almost same temperature. This justifies that the gelation occurs by the liquid−liquid phase separation due to concentration fluctuation of the solution. Namely, the solutions at elevated temperature are thermodynamically unstable and tend to incur phase separation. The gelation rate becomes faster as the measured temperature in Figures 3, 4, and 6 becomes lower.

Now, as described in Experimental Section, the gelation temperature was determined after keeping the solution for 1 h corresponding to the time scale for determining the gelation temperature. On the other hand, as shown in Figures 3, 4 and 6, the spinodal

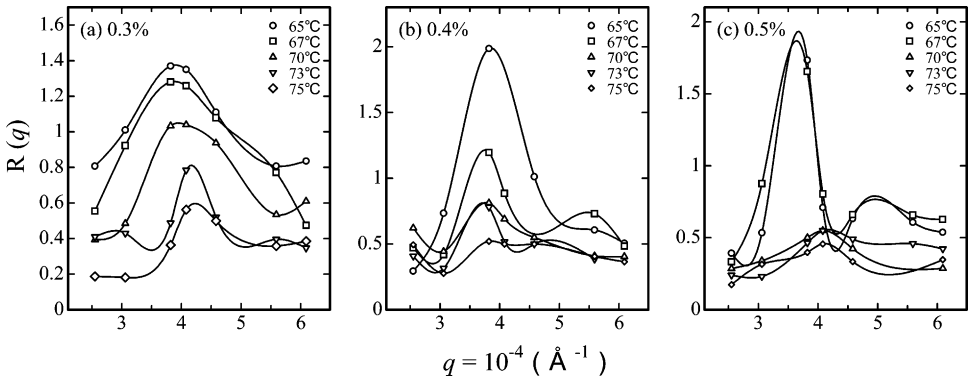

Figure 15. Growth rate of concentration $R(q)$ plotted against q estimated for the UHMWPE solutions with 0.3, 0.4, and 0.5% concentrations.

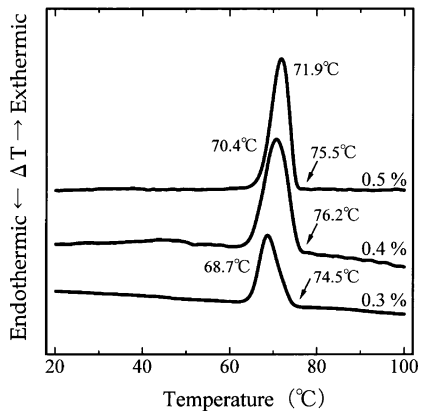

Figure 16. DSC curves for the UHMWPE solutions with 0.3, 0.4, and 0.5% concentrations.

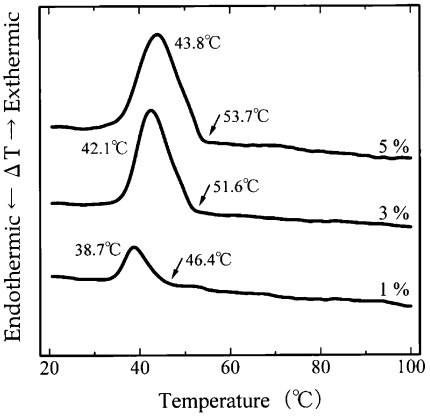

Figure 17. DSC curves for the B-LMWPE solutions with 1, 3, and 5% concentrations.

decomposition temperature is defined in the initial stage of spinodal decomposition corresponding to much shorter time scale than 1 h. If the gelation occurred at such a shorter time that the plots of ln(I) vs time tends to deviate from the linear relationship (see Figures 3, 4, and 6), it may be expected that the actual gelation temperature must be lower than the spinodal temperature listed in Tables 2 and 3. In this is the fact that the gelation temperatures of the UHMWPE and B-LMWPE solutions are postulated to be almost equal to their spinodal temperatures. This justifies that the liquid−liquid phase separation is a sort of driving force to cause gelation/crystallization, and then the crystallization occurs in the polymer-rich phase produced by the phase separation of the solution.

To check the above concept, the gelation time must be estimated at the temperature adopted for measuring the change in ln(I) against time in Figures 3, 4, and 6. In doing so, the falling ball method was adopted. The gelation time of the UHMWPE and B-LMWPE solutions becomes shorter with increasing concentration and with decreasing the measured temperature. For example, the gelation of the 0.3% UHMWPE solution kept at 75 °C occurred at ca. 2 min, denoting the beginning of the later stage. The same tendency was also confirmed for the rest solutions. This demonstrates that the gelation of the UHMWPE and B-LMWPE solutions occurs in the time scale, showing the deviation from the linear relationship of ln(I) vs t and the gelation surely occurred in the beginning of the later stage.

Certainly, the X-ray intensity in Figures 8 and 9 and scattered light intensity in Figures 3, 4, and 6 together indicate no crystallization in the initial stage of the phase separation of the UHMWPE and B-LMWPE solutions. Even so, we must emphasize that the gelation must be attributed to quasi-crystallites with such large fluctuation of crystal lattice distance as cannot be detected by X-ray diffraction technique. The quasi-crystallites must play an important role as cross-liking points to form gels, and this phenomenon can be estimated by correlation length associated with the extension of the inhomogeneties. If there were no cross-linking points, it is obvious that the physical gel cannot form.

For the B-LMWPE gels, Hv scattering showed no pattern at 5 min after quenching solution to 65 °C as shown in Figure 7, and the corresponding Vv scattering showed the circular pattern with no μ dependence indicating isotropic scattering. In this case, Vv scattered intensity can be written as follows:[36,37]

$$I_{\mathrm{Vv}} = K_2\langle\eta^2\rangle_{\mathrm{av}}\int_0^\infty \gamma(r)\,\frac{\sinh r}{h}\,r^2\,\mathrm{d}r \qquad (3)$$

where $\langle\eta^2\rangle$ is the mean-square polarizability fluctuation and $\gamma(r)$ is the corresponding correlation function. In the present study, the angular dependence of scattered intensity is assumed to be a monotonically decreasing function. Such a function is very difficult to obtain $\gamma(r)$ by a Fourier transformation with sufficiently accuracy. The desired information could be extracted by assuming that the scattering over the entire angular range can be described by a sum of Gaussian functions.[38] Then, we have

$$\gamma(r) = \exp\left(-\frac{r^2}{a^2}\right) \qquad (4)$$

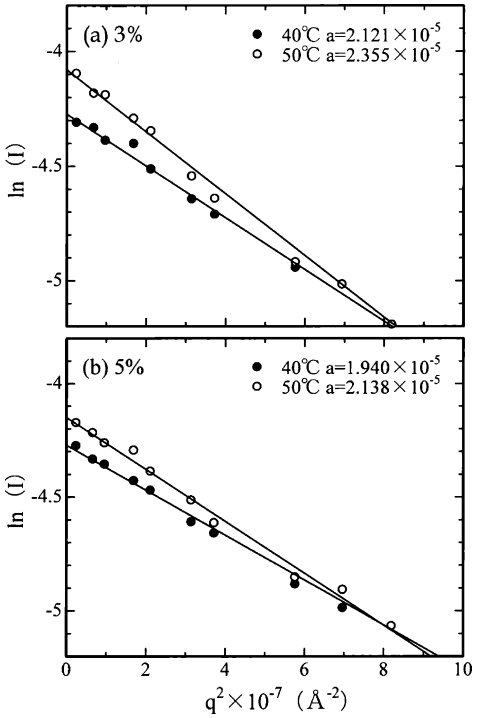

Figure 18. Scattered intensity data plotted as the logarithm of the absolute Rayleigh ratio vs q^2 for the B-LMWPE gels at 40 and 50 °C: (a) 3% solution, (b) 5% solution.

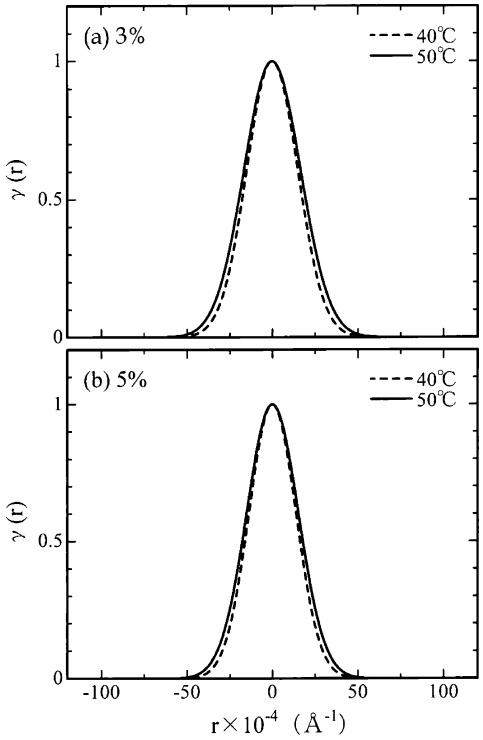

Figure 19. Correlation functions $\gamma(r)$ of the B-LMWPE gels at 40 and 50 °C: (a) 3% concentration, (b) 5% concentration.

The parameter a is the correlation length estimating the extension of the inhomogeneities. The gel becomes a uniform structure when a takes infinite.

Substituting eq 4 into eq 3 and performing the integration yields

$$\ln(I_{Vv}) = \ln\left(\frac{16}{\lambda^4}\pi^{11/2}\langle\eta^2\rangle a^3\right) - \frac{a^2}{4}q^2 \qquad (5)$$

Figure 18 shows scattered intensity data plotted as the logarithm of the absolute Rayleigh ratio vs q^2 for the 3 and 5% B-LMWPE gels prepared after quenching the solutions to 40 and 50 °C. The upper and lower columns are shown for the 3 and 5% concentrations, respectively. The measurements were done at ca. 3.5 min after quenching. The slope of the line allows the determination of the parameter a in eq 5, and by extrapolation to zero angle the quantity $\langle\eta^2\rangle$ is obtained.

By using the value of a, $\gamma(r)$ curves were recalculated, which are shown in Figure 19. The profile of $\gamma(r)$ for the 3% gel is broader than that for the 5% gel, since a is slightly longer as shown in Figure 18. At the same concentration, the profile of $\gamma(r)$ at 50 °C is slightly broader than that at 40 °C. This justifies that the number of cross-linking points in the polymer-rich phase of the solution increases with increasing the concentration and with decreasing the cooling temperature. This is probably due to the different growth rate of liquid−liquid phase separation, which is in good agreement with a series of experimental results in this paper. Unfortunately, the same analysis was difficult for the UHMWPE solutions because of the rapid appearance (45 s) of the Hv pattern as shown in Figure 5.[39]

In accordance with the previous work, it has been reported that when UHMWPE solution was quenched to temperature lower than 70 °C, which is lower than the spinodal temperature as well as the gelation temperature as listed in Tables 2 and 3, the resultant gels could form a uniform film after evaporating solvents. But the UHMWPE could not form a single-crystal mat despite linear polyethylene but the L-LMWPE could form,[40] since molecular chains of the UHMWPE are too long to form single-crystal mats.

When the UHMWPE and L-LMWPE blend film prepared by gelation/crystallization from solution was elongated, the X-ray diffraction pattern revealed different orientation modes of the HHMWPE and L-LMWPE crystallites, which was discussed already elsewhere by Bin et al.[19] They pointed out that the different crystallization modes under quenching process hamper cocrystallization, while the blends of UHMWPE and B-LMWPE can be elongated up to 200 times smoothly. The Young's moduli for the UHMWPE/B-LMWPE compositions = 1/1 and 1/9 reached 76.5 and 54.1 GPa, respectively.[19] The orientational degree of both crystallites were almost the same, indicating the cocrystallization under quenching process, which seems to reflect the similar gelation mode as discussed in this paper. This investigation indicates that the gelation mechanism of polyethylene, dependent upon the molecular weight and the degree of branching, plays an important role to produce the high modulus and high strength fibers with commercially speed, since the viscosity of solution undergoes a drastic decrease with increasing content of LMWPE.[31]

Certainly, it is obvious that the morphology and mechanical properties of the UHMWPE films were related to the characteristics of the phase separation of the solutions. Under scanning electron microscopy, the tissue in the film was observed to take a honeycomb-like structure,[39−41] whose hole size became smaller as the quenching temperature decreased.[39] The dense network structure was reported to be effective to transmit inner stress smoothly in the stretching direction.[34,35] This result was found to be almost the same as reported for UHMWPP.[17]

Conclusion

The gelation mechanism of three kinds of polyethylene (UHMWPE, B-LMWPE, and L-LMWPE) solutions was investigated by using elastic light scattering techniques in terms of phase separation due to concentration fluctuation of the solution. The logarithm of scattered light intensity from the UHMWPE and B-LMWPE solutions increased linearly with time in the initial stage of the liquid−liquid phase separation, when the solutions had been quenched to a desired temperature. This phenomenon could be analyzed within the framework of the linear theory of spinodal decomposition proposed by Cahn in terms of the phase separation of solution. This analysis was based on the concept that the UHMWPE and B-LMWPE solutions are quenched to temperatures lower than their gelation temperature, the solutions became thermodynamically unstable, and then they tend to incur phase separation to resolve the unstable state. In such supercooled solutions, any crystallites could not be detected by X-ray diffraction in the initial stage of the phase separation, ensuring the linear increase in the logarithm plots of the scattered light intensity against time. This result suggests that the gelation of the UHMWPE and B-LMWPE solutions is generated in the polymer-rich phase (the heterogeneous network system) occurred by the phase separation, and then the phase separation plays a driving force to cause gelation/crystallization. Of course, it is evident that there exist ordered structures like paracrystallites with large fluctuation of lattice distance in the initial stage, which cannot be detected by X-ray diffraction. Probably, the structure in the polymer-rich phase formed optically anisotropic rods or spherulites in the later stage of the phase separation. In contrast, the L-LMWPE solution became opaque rapidly by quenching the solution indicating the crystallization, but the crystallization was too rapid to obtain the refined results by scattered light intensity as a function of time.

References and Notes

(1) Kobayashi, M.; Nakaoki, T.; Ishihara, N. *Macromolecules* **1990**, *23*, 78.
(2) Kobayashi, M.; Kozasa, T. *Appl. Spectrosc.* **1993**, *47*, 1417.
(3) Kobayashi, M. *Macromol. Symp.* **1997**, *114*, 1.
(4) Tan, H.-M.; Moet, A.; Hilter, A.; Bear, E. *Macromolecules* **1983**, *16*, 28.
(5) Gan, J. Y. S.; Francois, J.; Guenet, J.-M. *Macromolecules* **1986**, *19*, 173.
(6) Klein, M.; Guenet, J.-M. *Macromolecules* **1989**, *22*, 3716.
(7) Klein, M.; Brulet, A.; Guenet, J.-M. *Macromolecules* **1990**, *23*, 540.
(8) Guenet, J.-M. *Macromolecules* **1986**, *19*, 1961.
(9) Boyer, R. F.; Baer, E.; Hiltner, A. *Macromolecules* **1985**, *18*, 427.
(10) Izumi, M.; Suzuki, J.; Katano, S.; Funahashi, S. *Physica B* **1995**, 213−214, 724.
(11) Pines, E.; Prins, W. *Macromolecules* **1973**, *6*, 888.
(12) Feke, G. T.; Prins, W. *Macromolecules* **1974**, *7*, 527.
(13) Nishi, T.; Wang, T. T.; Kwei, H. *Macromolecules* **1975**, *8*, 227.
(14) Kanaya, T.; Ohkura, M.; Kaji, K.; Furusaka, M.; Misawa, M. *Macromolecules* **1994**, *27*, 5609.
(15) Matsuo, M.; Kawase, M.; Sugiura, Y.; Takematsu, S.; Hara, C. *Macromolecules* **1993**, *26*, 4461.
(16) Matsuo, M.; Sugiura, Y.; Takematssu, S.; Ogita, T.; Sakabe, Nakamura, T. R. *Polymer* **1997**, *38*, 5953.
(17) Matsuo, M.; Hashida, T.; Tashiro, K.; Agari, Y. *Macromolecules* **2002**, *35*, 3030.
(18) Matsuo, M.; Tanaka, T.; Ma, L. *Polymer* **2002**, *43*, 5299.
(19) Bin. Y.; Fukuda, M.; Kurosu, H.; Matsuo, M. *Macromol. Symp.* **2000**, *147* 1.
(20) Bin, Y.; Ma, L.; Adachi, M.; Kurose, H.; Matsuo, M. *Polymer* **2001**, *42*, 8125.
(21) Sawatari, C.; Matsuo, M. *Polymer* **1989**, *31*, 1603.
(22) Smith, P.; Lemstra, P. J.; Kalb, B.; Pennings, A. J. *Polym. Bull. (Berlin)* **1979**, *1*, 733.
(23) Smith, P.; Lemstra, P. J. *J. Mater. Sci.* **1980**, *15*, 505.
(24) Smith, P.; Lemstra, P. J.; Pipper, J. P. L.; Kiel, A. M. *Colloid Polym. Sci.* **1981**, *258*, 1070.
(25) Usami, T.; Takayama, S. *Macromolecules* **1984**, *17*, 1756.
(26) Mori, S. *J. Appl. Polym. Sci.* **1974**, *18*, 2391.
(27) Mirabella, F. M.; Ford, E. A. *J. Polym. Sci., Phys. Ed.* **1987**, *25*, 777.
(28) Beer, F.; Capaccio, G.; Rose, L. J. *J. Appl. Polym. Sci.* **1999**, *73*, 2807.
(29) Rhodes, M.; Stein, R. S. *J. Polym. Sci., Part A-2* **1969**, *7*, 1539.
(30) Stein, R. S.; Rhodes, M. B. *J. Appl. Phys.* **1960**, *31*, 1873.
(31) Ogita, T.; Yamamoto, R.; Suzuki, N.; Ozaki, F.; Matsuo, M. *Polymer* **1991**, *32*, 822.
(32) Sawatari, C.; Okumura, T.; Matsuo, M. *Polym. J.* **1986**, *18*, 741.
(33) Cahn, J. W. *J. Chem. Phys.* **1965**, *42*, 93.
(34) Cahn, J. W.; Hilliard, J. E. *J. Chem. Phys.* **1958**, *29*, 258.
(35) van Aartsen, J. J. *Eur. Polym. J.* **1970**, *6*, 919.
(36) Deby, P.; Bueche, A. M. *J. Appl. Phys.* **1949**, *20*, 518.
(37) Stein, R. S.; Wilson, P. R. *J. Appl. Phys.* **1962**, *33*, 1914.
(38) Wun, K. L.; Prins, W. *J. Polym. Sci., Polym. Phys. Ed.* **1974**, *12*, 533.
(39) Ogita, T.; Kawahara, K.; Soga, K.; Matsuo, M. *Polymer* **1992**, *33*, 698.
(40) Ogita, T.; Kawahara, K.; Nakamura, R.; Ochi, T.; Minagawa, M.; Matsuo, M. *Macromolecules* **1993**, *26*, 4646.
(41) Matsuo, M.; Inoue, K.; Abumiya, N. *Sen-I-Gakkaishi* **1983**, *36*, 696.
(42) Matsuo, M.; Sawatari, C.; Iida, M.; Yoneda, M. *Polym. J.* **1985**, *17*, 1197.

MA058003P